Automated Reconstruction of Cast-off Blood Spatter Patterns based on Euclidean Geometry and Statistical Likelihood

(manuscript accepted November 23, 2020 by Forensic Science International)

The final version of the manuscript is available at https://www.sciencedirect.com/science/article/abs/pii/S0379073820304904

Citation:

S. McCleary, E. Liscio, K. De Brabanter, and D. Attinger, "Automated reconstruction of cast-off blood spatter patterns based on Euclidean geometry and statistical likelihood," Forensic Science International, vol. 319, p. 110628, 2021/02/01/ 2021.

The open-source software implementing the method is available at

https://github.com/scottres/CastoffReconstruction.git

Automated Reconstruction of Cast-off Blood Spatter Patterns based on Euclidean Geometry and Statistical Likelihood

Authors

Scott McCleary[1]; Eugene Liscio[2]; Kris De Brabanter[3]; and Daniel Attinger[4]

(1)
240 E Walnut St APT 108
Des Moines, IA 50309
Email: scott.thomas.mccleary@gmail.com

(2)
P. Eng.,
ai2-3D
271 Jevlan Drive, Unit 14
Woodbridge, Ontario
L4L 8A4
Canada
Email: eliscio@ai2-3d.com

(3)
Iowa State University
Department of Statistics
2419 Snedecor Hall
2438 Osborn Dr.
Ames, IA, 50011-1210
and
Department of Industrial Manufacturing & Systems Engineering
3033 Black Engineering
2529 Union Dr
Ames, IA 50011-2030
Email: kbrabant@iastate.edu

(4)
Department of Mechanical Engineering,
Iowa State University, 2025
Black Engineering,
Ames, 50011, IA
and
Struo LLC
Ames IA 50010
United States of America
Email: Struo.Attinger@gmail.com (corresponding author)

Abstract

Cast-off spatter patterns exhibit linear trails of elliptical stains. These characteristic patterns occur by centrifugal forces that detach drops from a swinging object covered with blood or other liquid. This manuscript describes a method to reconstruct the motion, or swing, of the object. The method is based on stain inspection and Euclidean geometry. The reconstructed swing is represented as a three-dimensional region of statistical likelihood. The reconstruction uncertainty corresponds to the volume of the reconstructed region, which is specific to the uncertainties of the case at hand. Simple numerical examples show that the reconstruction method is able to reconstruct multiple swings that are either intersecting or adjacent to each other. The robustness, spatial convergence, computing time of the reconstruction method is characterized. For the purpose of this study, about 20 cast-off experiments are produced, with motion of the swinging object documented using video and/or accelerometers. The swings follow circular or arbitrary paths, and are either human- or machine-made. The reconstruction results are compared with the experimentally documented swings. Agreement between measured and reconstructed swings is very good, typically within less than 10 cm. The method used in this study is implemented as a numerical code written in an open source language, provided in an open access repository, for purposes of transparency and access.

Introduction

Cast-off spatters often occur during crimes involving beating events. In the context of bloodstain pattern analysis, a c*ast-off spatter pattern* is defined as "*a bloodstain pattern resulting from blood drops released from an object due to its motion*" [1]. *Cast-off* spatters occur when non-gravitational inertial forces overcome the capillary forces retaining blood on an object experiencing linear or rotational acceleration. In the latter case, the inertial forces are called centrifugal forces. Cast-off patterns are characterized with linear or curvilinear stain distributions [2]. Cast-off patterns tend to be elongated, as compared to impact spatter that exhibit radial dispersions as shown in Figure 1(c) [3]. Other occurrences of cast-off spatters involve water or mud projection by vehicle wheels. The scope of this manuscript is focused on spatters relevant to bloodstain pattern analysis.

The dynamics of cast-off formation have been well documented [2, 4-9]. Blood adhering by capillary forces on a swinging object detaches when centrifugal forces become large enough to balance capillary forces. The detaching drops leave the swinging object tangentially to its swing, with an initial velocity equal in magnitude and direction to that of the weapon at the instant of detachment. The trajectories of the drops are then controlled by gravitational and drag forces. They can be described with Newton's second law of motion. While several studies have described the reconstruction of *impact* spatter patterns [10-15], where the area of origin of the blood is assumed to be static, there is currently no available method to reconstruct the trajectory of the swinging object that generates a *cast-off* spatter pattern. Current reconstruction methods for impact spatter patterns are called *method of strings* or *tangent method*, assume the blood drops travel in straight trajectories from the impacted blood source to the stain impact locations. The method presented in this manuscript is about reconstructing the swing of the object causing the spatter pattern, based on stain inspection and statistical methods.

Studies on cast-off patterns have also produced reconstruction guidelines [2, 4, 16]. Recent advances in theory, measurement, and crime scene processing have shed light on various aspects of cast-off patterns [2, 16, 17]. Two studies, by Maloney [17] and Liscio [16], propose methods for the analysis and interpretation of cast-off patterns. Method [17] results in the determination of an "*approximate plane*

of motion", a plane within which the bloody weapon has probably swung. This *plane of motion* is calculated using least squares and orthogonal regressions [17]. Method [16] presents and determines a "*path volume envelope*" (§10 [16]) that encloses the weapon swing. The *path volume envelope* is a box "defined as the space which contains all or part of the object path which created the cast-off stains" (§8 in [16]). The method in [16] also defines an "*exclusion zone*" , that is a volume where the cast-off spatter pattern is not likely to have originated. Both methods result in a plane containing the reconstructed motion of the weapon swing, which is supposedly planar. The error associated with these methods can be estimated as the distance between the plane, or associated planar region, and the known cast-off swing motion. Human created cast-off patterns, commonly present on crime scenes, are not necessarily planar [2], and might involve multiple swings.

To date, there are no methods to directly reconstruct the swing(s) of a weapon from inspection of cast-off spatter patterns. In this manuscript, we develop a geometric and statistical reconstruction method. The geometric approach determines circular segments of the weapon swing from triplets of stains, which are then assembled statistically to reconstruct weapon swings featuring variable radii and multiplanar motion. The reconstructed swing is represented statistically with uncertainty regions [12], which are volumes of arbitrary shape that are likely to contain the swing of the weapon. Analog probabilistic approaches have been proposed for the reconstruction of impact spatter patterns by Camana [12] in 2D and then by Attinger et al. in 3D [18]. The methods involve the propagation of measurement uncertainties and the construction of a joint probability density function (PDF) [18]. The method in this manuscript is analog, in the sense that similar statistical methods are used, however the reconstruction results is the path of a bloody weapon rather than a stationary blood source.

1. Experiments

Figure 1 shows the three setups used to produce cast-off patterns to develop and test the reconstruction method. One set of cast-off spatter patterns was conducted with a sitting participant who swung a wet rod around his shoulder, and two sets of patterns were produced by circular and non-circular motions of a wet rod. A total of about 20 spatter patterns was used to develop and test the reconstruction method.

1.1. "Sitting" cast-off spatter patterns

Four cast-off spatter patterns were created by the first author, who swung a wooden rod while seating, as shown in Figure 1. Fluid was ink solution (Royal Talens Amsterdam green and red acrylic ink) diluted with an equal volume of deionized water, and later swine blood. Swine blood trials were conducted at room temperature, 22 ± 1 ℃, with ethically-sourced blood containing approximately 1 % heparin to prevent coagulation. Swine blood was chosen to minimize biohazards, and is a substitute to human blood with similar physical properties [5, 19, 20]. The blood was drawn less than 24 hours prior to experimentation and stored under refrigeration and on a rocker. Hematocrit was measured within the range of 44-48 % prior to experimentation with a dedicated centrifuge device (STI, Hemata-Stat-II). The blood was warmed to room temperature while on a rocker before experimentation. The reconstruction method proposed in this manuscript is independent on the fluid properties which explain why the first trials, done early in the training of the first author, were not done with blood. The wooden rod was dipped in a 25 mL beaker containing a 15 mL ink solution or swine blood to produce cast-off spatter

patterns. The seated position was used to maintain a constant center of rotation, approximately around the shoulder.

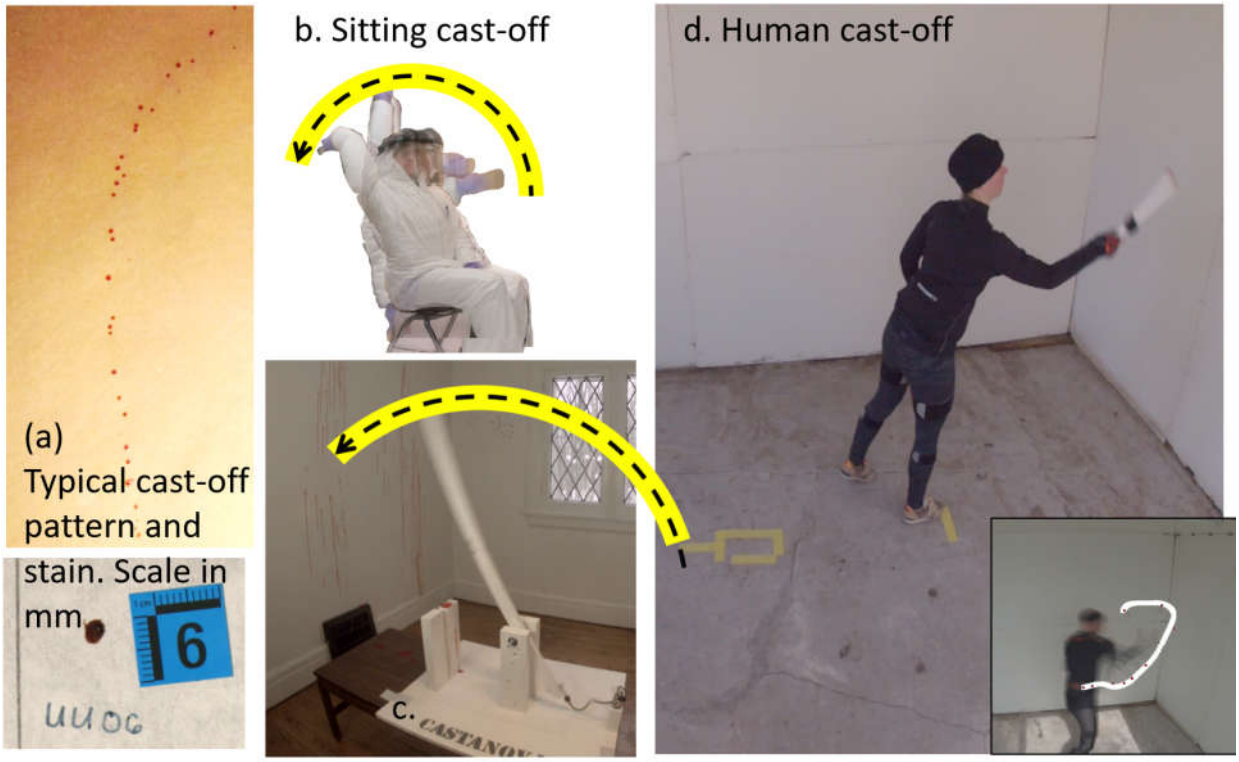

Figure 1: Cast-off spatter patterns such as (a) have been generated in three ways: (b) participant *sitting* and rotating his arm, with measured weapon swing indicated in dashed black arrow. (c) using a *Castanova* rig, where wooden arm rotates around fixed axis driven by bungee cord, with measured swing motion as dashed black arrow; and (d) *human* participant creating a cast-off pattern during downward swing. Reference markers on the floor help calibrate motion measurement, and position trackers are mounted on the participant and on the bloody rod. The inset shows overlaid experiment video frames with the captured motion (in white). Tip of rod for each video frame is highlighted as visual assistance.

The experiments were conducted in an enclosed room with dimensions (*X, Y, Z*)=(248 cm, 159 cm, 243 cm)[21]. The swinging motion was in a vertical plane. The swing radius was about 70 cm. Stains were spattered onto the front, back, ceiling, and ground surfaces, which were covered with butcher paper. Stains were individually imaged at approximately 200-250 DPI with a DSLR camera (Canon EOS 70D) with a plumb line and measurement 10 ± 0.2 mm reference marker with manufacturer uncertainty tolerancing (KISS System WMM50B Wound Mapping Marker). Stain locations were measured with a square ruler referencing the defined origin room corner. Stain images were analyzed using HemoSpat® to determine stain width, length, and impact angles [14], as illustrated in Figure 2. The uncertainty on the weapon swing was estimated as a radius of 5 cm.

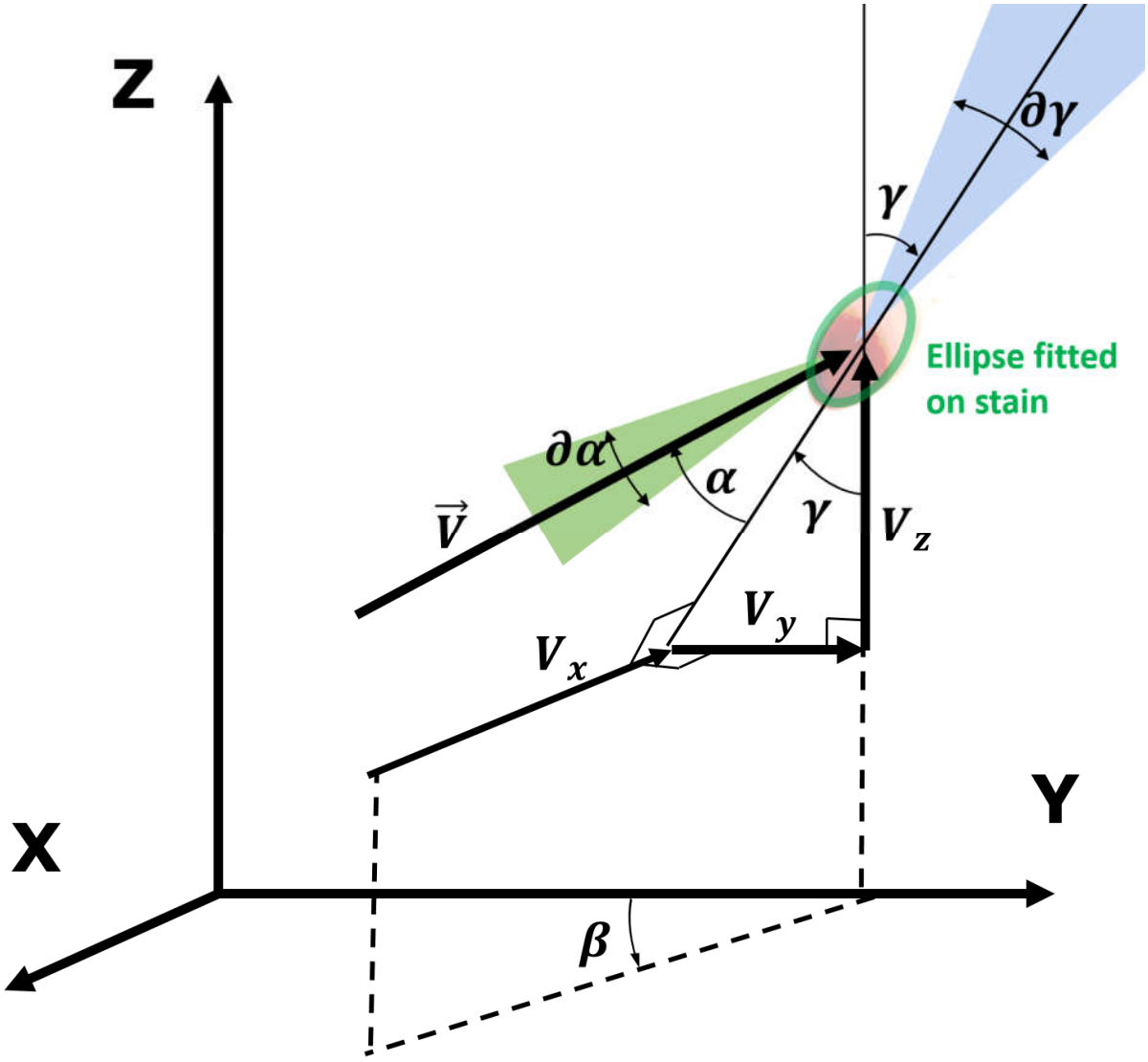

Figure 2: Impact angle α, directional angle γ, and angle β are determined from inspection of stain ellipticity and directionality. Symbols $\delta\alpha$ and $\delta\gamma$ are the uncertainty on the estimated direction of the respective impact velocity and of the main axis of the stain. Drop impact vector $\vec{V}$ is shown with its three components V_x, V_y, and V_z [13]. Coordinates *XYZ* are global coordinates.

1.2. Cast-off spatter patterns from the "Castanova" rig

Ten spatter patterns with the constant radius "Castanova" mechanical cast-off rig were performed as described in [22], with method summarized here. An amount of $5mL$ of sheep blood at 23 ± 1 ℃ was deposited to the end of a wooden arm affixed with a 3D printed sphere with diameter of 4 cm. Hematocrit for sheep blood ranges between 13 and 32 % [23]. The arm was able to rotate around a fixed axis, was drawn back with a bungee cord and released to produce the cast-off spatter. The swing motion was constrained in a vertical plane and spatter stains were produced mostly on the front wall. The experiments involved pattern generation, identification, bloodstain labeling and photographing, laser scanning (here FARO Focus S350 with ranging error of ± 1 mm and angular accuracy of 19 $arcseconds$),

with reference markers on the wall. Data analysis in a computer aided design (CAD) program (FARO Zone 3D) was used to align stain photographs with a three-dimensional representation of the room. Results were displayed by importing all data into 3ds Max [22]. The cast-off rig produced five trials at $0.5m$ and another five trials $1.0m$ from the target surface [22]. The velocity of the cast-off producing end of the member after the trials was approximately $10.5 \pm 1.2 \ \frac{\mathrm{m}}{\mathrm{s}}$ [22]. A detailed three-dimensional analysis of the experiments is available in [22]. The uncertainty on the weapon swing was estimated as a radius of 2.7 cm.

1.3. "Human", non-circular cast-off spatter patterns

Six cast-off patterns were generated by a human participant swinging a wooden rod in a non-circular trajectory representative of an actual fight ("Human cast-offs" #1-4, 6-7). The documentation and measurements process of the stains was same as with the *Castanova* rig. In the experiments, the blood was previously donated from volunteers, and spiked with anticoagulant. The blood was heated to room temperature (approximately $23\ ^{\circ}\mathrm{C}$) prior to use.

The motion of the weapon relative to the bloodstained surfaces was measured and documented as follows. Eighteen accelerometer and gyroscope systems were used (MTw Awinda from Xsens [24]). This motion capture system is a commercial motion capture system with six degrees of freedom (linear accelerations along (*X, Y, Z*) coordinates axes and rotational accelerations along three perpendicular (ϕ, θ, ψ) orientations). The motion capture system determines the $(\mathrm{X}, \mathrm{Y}, \mathrm{Z})$ coordinate locations from the linear and rotational accelerations. The measurement setup allows for eighteen body motion trackers placed at various areas on the body and one additional tracker fixed on the item being used as a "weapon".

The weapon used for this study was a wooden rod with a length of 34 cm and a diameter of approximately 4cm. A tracker was placed on the rod, fixed at a known position along the length of the rod at approximately 10 cm from the end held by the subject. To reconstruct the motion of the end of the rod, the tracker data is translated by the corresponding length and oriented. The motion capture system requires that the person being recorded is "calibrated" in the system by entering their body dimensions and then by moving through a routine of prescribed motions that accurately calibrate each tracker to their respective position on the subject.

The motion recording began with the right foot of the participant aligned onto a reference marker on the ground. The participant then wet the rod by dipping into a small bowl of blood. Participants were directed to take a few steps towards the wall directly in front of them and then swing the rod with enough force to create a cast-off pattern. The motion started with the arm lowered, then raised up, then quickly downwards. Once the striking motion was complete, the subject was asked to step back and reposition their right foot on the marker. The recording was then ended. A total of six trials were recorded, all of which are used in this manuscript.

In addition to the motion capture system, a Microsoft Kinect sensor was used to record motion point cloud data of the subject creating the cast-off pattern [25, 26]. This was used as a redundant external system of a color CGA video camera in RGB and an infrared projector with 640×480 pixel resolution at 30 frames per second. The system allowed for the walls, floor, and motion of the subject to be captured in the global scale of the room. The motion capture system did not have any external references and

thus, having the participant place their right foot on a known marker at the beginning and end of each trial was used to accommodate for any drift or other possible inaccuracies in the motion capture system.

Based on the above setup, it was possible to align all the data such that the motion of the rod was measured in relation to the rest of the room during the generation of the cast-off pattern. The uncertainty on the weapon swing was estimated as a radius of 5.4 cm.

2. Theoretical reconstruction of cast-off patterns

2.1. Geometric reconstruction of segments of the weapon swing:

The proposed reconstruction method is based on the fact that drops leave the weapon tangentially to its trajectory and on the assumptions that (1) the trajectories of the drops are linear, along a line that contains the stain of interest, with slope estimated from stain inspection and (2) that the weapon follows a circular trajectory, at least over small displacements (piecewise circular swing).

Under these two assumptions, each circular piece of the swing can be reconstructed as in Figure 3. To do so, we use a geometrical property of triangles adjacent to a circle, as in Proposition 4 of book IV of the Elements by Euclid. Euclid lived in the third century before the Common Era and is considered the founder of geometry. To the best of our knowledge, he did not produce any work on forensics, unlike his younger contemporary Archimedes who is credited with uncovering commercial fraud by applying the buoyancy laws [27] that he discovered. In the application of Euclidean geometry proposed here, the green circle describes the trajectory of the weapon, and the adjacent triangle (A, B, C) is formed by intersections of the trajectories of three blood drops, reconstructed from stains *M, L, N*. In his proposition **§**127, Lachlan [28] shows that Euclid's work implies that "The internal bisector of the angle BAC, and the external bisectors of the angles ABC, ACB, are concurrent. Let the point in which they meet be denoted by I_1. This point is the centre of a circle which can be drawn to touch the sides of the triangle, but it is on the side of BC remote to A. This circle is called an *escribed circle* […] L_1, M_1, N_1 be the points of contact of the sides with this circle".

In the forensic reconstruction task at hand, the escribed circle proposition is valid for any set of three stains with trajectories of the associated drops are not parallel, such as the set labelled M, L, N in Figure 3. Using this proposition, triplets of three adjacent stains will typically determine an escribed circle along which the swinging weapon is most likely to have travelled. More precisely, the arc shown in magenta in Figure 3 connects the three points of contact of the stain trajectories with the escribed circle, and best approximates the likely reconstructed weapon swing. Then, the various arcs produced by various triplets of stains are combined in the probabilistic manner described below, so that circular and non-circular curves of swinging weapon can be reconstructed.

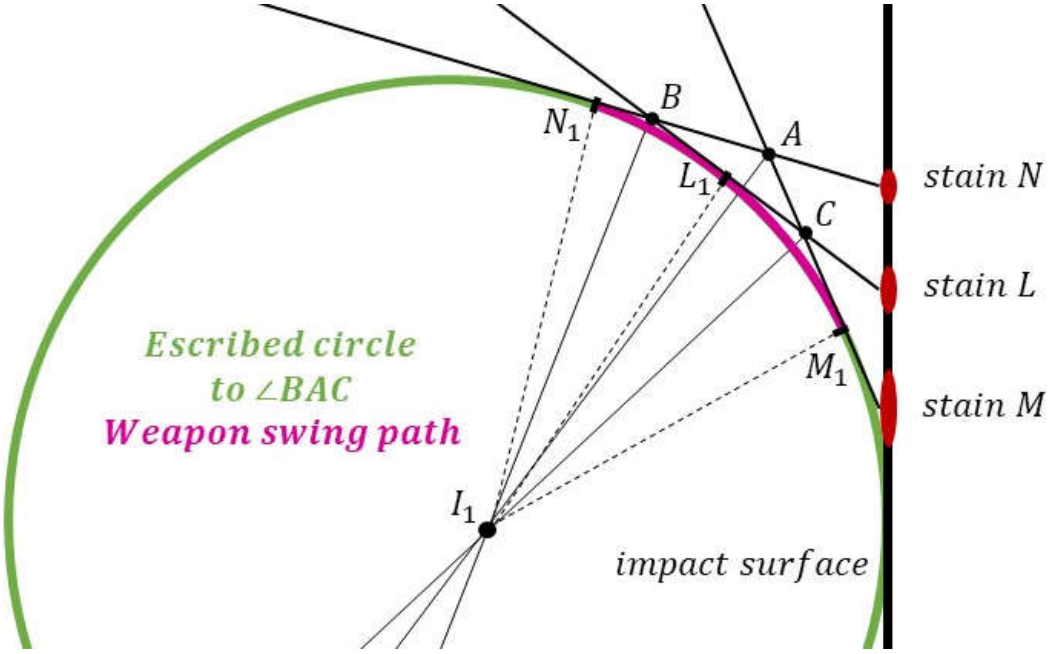

Figure 3: Escribed circle to $\angle BAC$ for stain trajectories derived from stains M, L, N. The points of contact of the stain trajectories with this circle are M_1, L_1, N_1 containing the weapon swing arc.

2.2. Probabilistic reconstruction of the weapon swing:

The geometric reconstruction approach above produces multiple segments in the form of arcs. A probabilistic approach has been developed to achieve two tasks: adding a specific thickness to the reconstructed arcs based on the propagation of measurement uncertainties (the thickness being a representation of the uncertainty in determining the swing motion) and merging the arcs obtained from all the reconstructed triplets/triplets of stains into a volume that reconstructs most of the swing of the weapon. Each reconstructed arc has the appearance, visually and culinary speaking, of a *noodle*. The centerline of the noodle describes the most likely arc associated with a triplet of stain, and the thickness of the noodle, the associated uncertainty. The volume merged from all the arcs may assume any shape based on the probabilistic union of multiple arcs with given thickness.

Based on the principle of maximum likelihood estimation, the uncertainty of the reconstructed arc is expressed probabilistically, in a manner analogous to what Camana [12] and Attinger et al. [18] have done for impact spatter patterns (the simpler situation where the blood source is assumed to be immobile). In the present case, we assume that the uncertainty of any measurement relevant to the reconstruction process can be expressed as a probability density function (PDF), Eq. (1), where μ is the mean of the measurement, σ_k is the standard deviation, and x is a continuous random variable, such as an angle or a distance:

$$\psi_k(x) = \frac{1}{\sigma_k\sqrt{2\pi}} e^{-\frac{1}{2}\left(\frac{x-\mu}{\sigma_k}\right)^2}. \qquad \text{Eq. (1)}$$

The space considered in the analysis is the room containing the blood spatter pattern. It is discretized with a Cartesian grid into uniform cubic regions. As shown in Figure 4, the relative position of any given

spatial region is expressed with respect to the reconstructed arc using the radial distance Δ_{jn} between the center of a cube *j* and reconstructed cast-off arc *n*. In these symbols, index j represents a given region in space, and index n refers to the cast-off arc segment reconstructed from the *n*-th triplet of stains as per method in Figure 3. The radial distance is used as the continuous variable in Eq. (1) to estimate the relative likelihood that any given discretized region contains the reconstructed cast-off segment.

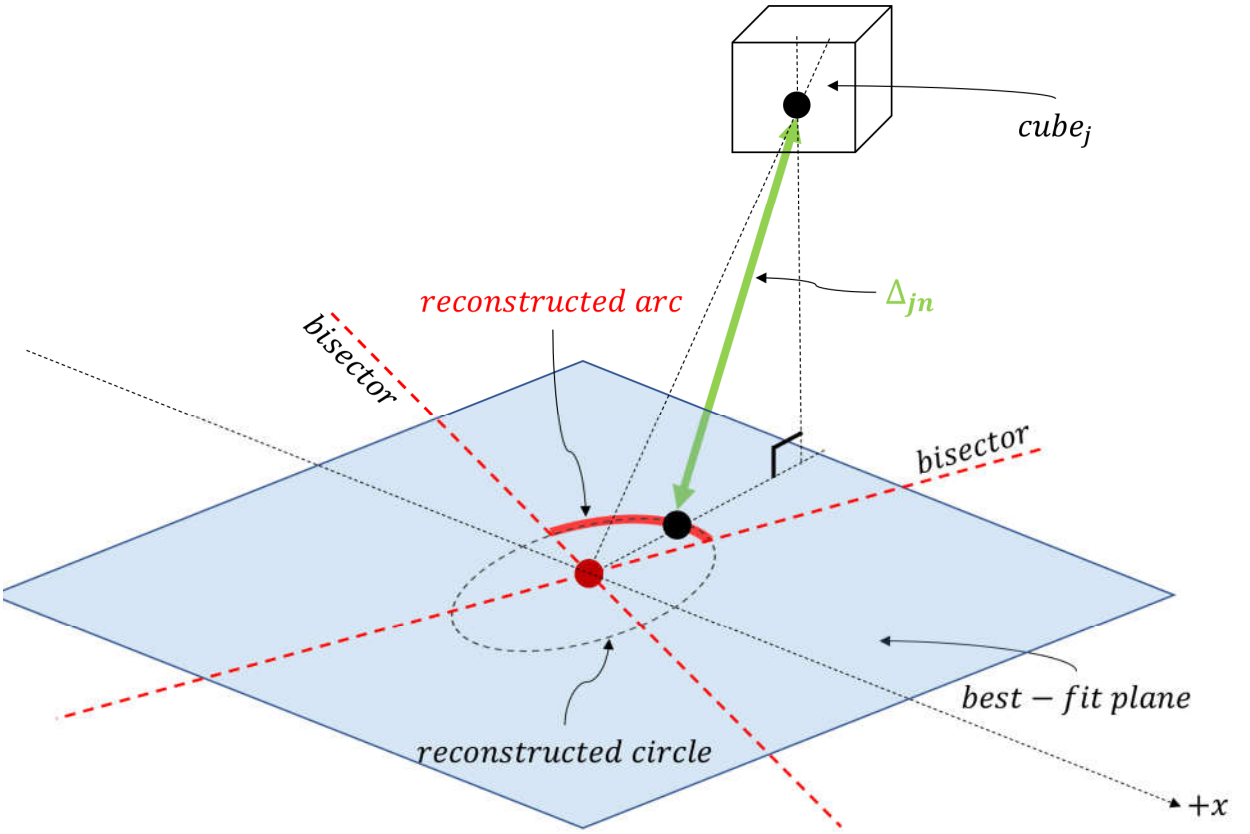

Figure 4: Geometry used for the reconstruction of a cast-off arc. The clustered mean plane is a best-fit plane to the triplet *n* of drop trajectories considered and contains the reconstructed arc (in red). The distance between a spatial region *jn* and the arc *n* is measured with (green) distance Δ_{jn}. Colors available in online version.

The probability that a given point in space is associated with a cast-off arc reconstructed from an arbitrary set of three stains can be quantified with the PDF

$$\psi_{jn} = \frac{1}{SF_{jn}\cdot\sqrt{2\pi}} e^{-\frac{1}{2}\left(\frac{\Delta_{jn}}{SF_{jn}}\right)^2} \quad \text{Eq. (2)}$$

As shown in Figure 5, this PDF is maximum for $\Delta_{jn} = 0$, which gives most weight to spatial regions coincident with the reconstructed arc. By definition of a normal distribution, the term SF_{jn} , in cm, is a spreading parameter that controls the shape of the distribution. Small spreading values correspond to very local distributions, while larger spreading values spread the distribution over larger distances. To

define the spreading value, we postulate that it depends on three independents quantities, graphically represented in the inset of Figure 5. We define

$$SF_{jn} = f(\overline{\alpha}, \overline{\varphi}, \Delta_{wall}), \qquad \text{Eq. (3)}$$

a function of the following variables: $\overline{\alpha}$, a measurement of the angular uncertainty associated with the triplet of stains associated with a reconstructed arc; $\overline{\varphi}$, an angle measuring the alignment of the three impact velocities associated with the triplet of stains and the best-fit plane containing the reconstructed arc; and Δ_{wall}, a measure of the distance between the triplet of the stains and the reconstructed arc. It is expected that function *f* in Eq. (3) increases monotonically with the increase of each of the three variables $\overline{\alpha}, \overline{\varphi}, \Delta_{wall}$. Indeed, a reconstructed arc will be known more accurately if there is little angular uncertainty in the related drop impact; if the directionalities of the stains align in the same plane; and if the reconstructed arc is close to the stained wall. A full definition of SF_{jn} is provided in Supplementary Documentation, and eight numerical examples of the related PDF ψ_{jn} are plotted in Figure 5. In short, the spread SF_{jn} is the product of the angular uncertainty of the stains in the triplet considered, and the average distance between the reconstructed arc and the stains. This way, the contributions of arcs reconstructed with higher accuracy are more significant (less spread-out) than those of arcs involving more uncertainty in their position. The PDF of Eq. (2) represents the likelihood that a region in space is associated with a reconstructed cast-off arc *n.*

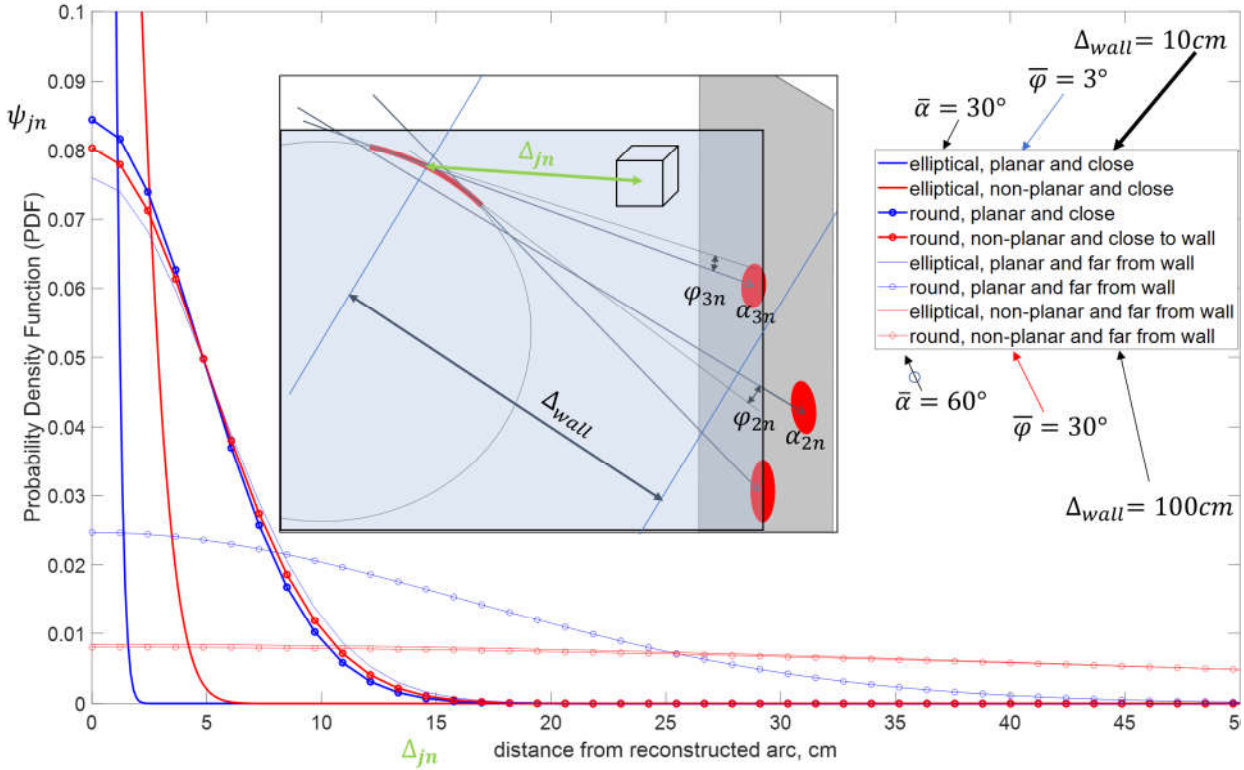

Figure 5: Shapes and values of PDF distributions corresponding to various types of stain triplets. The spread SF_{jn} and height of the PDF depends on angular uncertainty of stain measurement (here represented by $\overline{\alpha}$), alignment of the stains with the plane of the reconstructed arc $(\overline{\varphi})$, and on the distance Δ_{wall} between the reconstructed arc and the stains. The most important PDFs for reconstruction are narrow and correspond to triplets of stains that are elliptical, well aligned with the plane of the reconstructed arc, and close to that arc.

The likelihood that a region in space is associated with a cast-off event is then obtained as the product of the PDFs associated with each triplets of stains, as per Eq. (4), with *N* triplets.

$$\psi_j = \prod_{n=1}^{N} \psi_{jn}. \qquad \text{Eq. (4)}$$

Finally, the uncertainty U_L of a reconstruction is simply measured as the volume in space where the value of ψ_j is larger than an assumed likelihood value. For instance, $U_{75\%}$ is the uncertainty of a cast-off reconstruction assuming a likelihood value *L*=75 %. Uncertainty U_L has units of volume, for example liter (L).

3. Numerical and software implementation of the theoretical cast-off reconstruction model

3.1. Choice of software, scene processing and input data

The reconstruction model presented above is implemented as a software script that runs with Octave [29]. Octave is a free, open-source language generally compatible with Matlab®, a commercial scientific computing environment widely used in academia. The choice of Octave was made to address the common problem that forensic practitioners and other engineers rarely have commercial licenses of Matlab®. The software script has been checked to also be compatible with Matlab®. To reconstruct a spatter pattern, the inputs in Table 1 are similar to those required for existing impact spatter patterns reconstruction software, such as Hemospat®.

Project	Stain	**Location x**	**Location y**	**Location z**	Surface	**M axis (mm)**	**m axis (mm)**	**alpha**	**gamma**
castoff_2019_06.21	UF01	**250**	**35.9**	**93.8**	Back Wall	**3.3**	**3.2**	**73.8**	**60.4**
castoff_2019_06.21	UF02	**250**	**36.5**	**117.7**	Back Wall	**3.5**	**3.5**	**79.8**	**-16.6**
castoff_2019_06.21	UF03	**250**	**34.9**	**129.8**	Back Wall	**3.2**	**3.1**	**77.5**	**21.4**
castoff_2019_06.21	UF04	**250**	**42.5**	**170.6**	Back Wall	**4.2**	**3.7**	**62.4**	**11.8**
castoff_2019_06.21	UF05	**250**	**46.4**	**194.9**	Back Wall	**4.2**	**3.1**	**48**	**-0.2**
castoff_2019_06.21	UU06	**196**	**64.6**	**243**	Ceiling	**3.9**	**3.4**	**62.7**	**15**
castoff_2019_06.21	UU07	**145.8**	**65.9**	**243**	Ceiling	**3.1**	**2.9**	**70.2**	**72.8**
castoff_2019_06.21	UU08	**55.2**	**58.1**	**243**	Ceiling	**3.7**	**3.1**	**57.4**	**171.8**
castoff_2019_06.21	UU09	**38.8**	**54.8**	**243**	Ceiling	**3.1**	**2.3**	**48.2**	**167.8**
castoff_2019_06.21	UU10	**22.8**	**52**	**243**	Ceiling	**2.7**	**1.6**	**37.2**	**177**

Table 1: Example of user data inputs for the cast-off reconstruction software, required inputs are bolded. Global origin defaults to $(0,0,0)$ and room dimensions are extracted from XYZ-location coordinates.

Inputs required are room dimensions, the area of investigation defined by four walls (floor, ceiling and two vertical walls); normal unit vectors, by convention oriented outside of the room of the walls considered; tangential vectors to the walls considered (coplanar vectors to each wall in the direction of gravity unless walls are orthogonal to gravity in which case tangential vectors are defined in the positive *x*-direction); a global origin (to define an *XYZ*-coordinate system as shown in Figure 2; stain locations (*XYZ* component positions of the stain in centimeters relative to the origin location); stain directional angle γ, defined as the stain glancing angle between the projected trajectory vector onto the impacted surface and the tangent vector to the surface, and stain impact angle alpha α, the stain impact angle between the trajectory vector and the impacted surface as shown in Table 1. Inputs mentioned above

are entered by the investigator in the input file in order observed along the curvilinear cast-off patterns, in a comma-separated spreadsheet. A script, also called driver, formats and converts that spreadsheet units into data with format compatible with main software script.

3.2. Description of the reconstruction software

Determination of impact velocities: The yawing angle $\beta = \arctan\left(\frac{tan(\alpha)}{sin(\gamma)}\right)$ in Figure 2 is calculated from the α and γ impact angles [13]. Euclidean vector components are defined for each surface to describe stain impact angles in a global reference frame, surface definitions included in supplementary documentation.

Geometric reconstruction of individual cast-off arcs: Using the geometric reconstruction method presented in section 2.1, three escribed circles are defined on the triangle formed by the three converging drop trajectories [30] of a triplet of stains. To provide a best guess for which of these three circles is relevant to the cast-off swing, we use the Pratt fit method. The Pratt fit method is a curve fit method that algebraically fits a circle to data points [31]. The Pratt fit method determines a fitted circle center to be used as an approximated escribed circle reference point $[x_{ref}, z_{ref}]$, and this information is used to select the appropriate escribed circle, and apply the Euclidean theorem in section 2.1 to reconstruct the cast-off swing. More details on the Pratt fit method are in the Supplementary Documentation.

While Euclid's escribed circles theorem (section 2.1) is defined in a single plane, the drop trajectories of any triplet of identified stains are not necessarily in the same plane (while being approximately in the same plane, which results in the linear aspect of the pattern characteristic of cast-offs). To apply Euclid's theorem, we project the trajectories associated with the three stains of the triplet onto the best possible plane. This plane that we call the *best-fit plane* is the plane that minimizes the alteration of stain trajectories of the tree stains considered in each triplet. The best-fit plane is defined by a normal unit vector $\tilde{n}$ that minimizes the projection alterations (it minimizes its dot product with the stain trajectory vectors). This minimization task is done with either the Nelder-Mead [32] or Levenberg-Marquardt algorithm, with the Y-axis as initial guess. Vector $\tilde{n}$ and the point closest to the three stain determine the best-fit plane. Stain locations and their respective drop trajectories vectors are then translated and rotated onto the *XZ*-plane to reduce the stain trajectory intersections to a two-dimensional problem.

Typical reconstruction cases involved between *N*=5 to 100 triplets of stains. Given the narrow distributions of the PDFs in Eq. (2), and their *N*-time multiplication as per Eq. (4), there is a risk that the likelihood associated with a given region of space becomes zero during the reconstruction process, because of the finite numerical resolution of the computer performing the calculation. To avoid such artificial loss of data, the PDFs of individual triplets of stains are truncated to be at least as large as their 3-σ value, and the product of likelihood in Eq. (4) is rescaled as the computation proceeds. For reconstructing cast-off arcs, we could select every distinct combination of stain triplet $\binom{N}{3} = \frac{N!}{3!(N-3)!}$, less the triplets exhibiting at least two stains with parallel trajectories, for which there would no intersection of bisectors. Each triplet of non-parallel trajectories determines one triangle with 3 escribed circles. The escribed circle with center closest to $[x_{ref}, z_{ref}]$, identified with the Pratt-fit method, would provide an arc of the castoff, and its center, using the Euclidean geometric theorem above. However, we

found that the recorded swings were reconstructed in the most robust manner by selecting only the triplets of stains located close to each other, with approximately equal spacing along the stains. Selecting the triplets that way ensured that not only the circular swings, but swings of arbitrary trajectory shape would be reconstructed.

Results and Discussion

In this section, reconstruction results are described. The reconstructed patterns involve from actual cast-off experiments, and simulated cast-off patterns. The actual cast-off experiments include swings executed along circular and non-circular swings by human participants, and circular swings executed by the rotating arm of a *Castanova* device, already presented in [16].

Reconstruction results are presented in terms of uncertainty regions, which are spatial regions most likely to contain some of the path of the weapon that generated the cast-off. The uncertainty regions are estimated based on the geometric and probabilistic methods expressed above. Three embedded uncertainty regions are typically shown, each corresponding to a specific likelihood value. The likelihood value mathematically corresponds to the measure of goodness of a statistical fit and can assume values between zero and one. Practically, likelihood values of 60 %, 75% and 90% are used in this work. Low likelihood values correspond to larger uncertainty volumes and higher chances of intersecting the weapon swing. High likelihood values correspond to smaller uncertainty volumes and lower chances of intersecting the weapon swing.

For example, Figure 6 displays reconstruction results for a "Castanova" spatter pattern, where the motion of the blood-covered rod is circular. Several orthonormal views are presented of the uncertainty regions and measured weapon swing. Orthonormal views confirm that the reconstructed swing intersects with the measured swing, and measure the uncertainty of the reconstructed swing (which is represented by embedded regions of different likelihood). For instance, the green volume in Figure 6, $U_{75\%}$, is the uncertainty on the reconstructed cast-off swing assuming a likelihood value of 75 %. A spatial resolution of 5cm is used for all the numerical results presented in this work, unless specified otherwise.

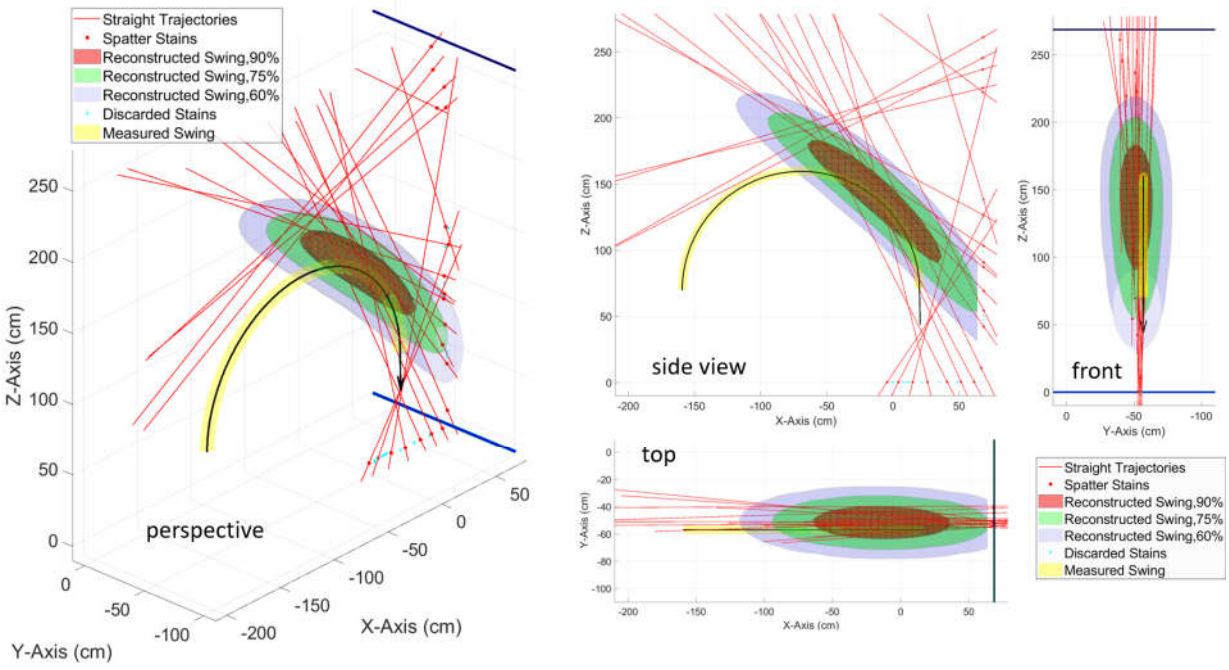

Figure 6: Reconstruction of the weapon swing in "Castanova" spatter pattern #10, seen from different viewpoints. The reconstructed swing is the red, green, or blue volume (respectively corresponding to likelihood of 90%, 75% or 60%), and intersects the measured cast-off swing (black arrow, with measurement uncertainty in yellow).

The results of one of the "*Sitting*" cast-off pattern, with experimental details described above, are presented in Figure 7. The measured swing of the ink-covered rod intersects the reconstructed swing. Figure 7 also illustrates the effect of the spatial reconstruction on the quality of the results. Results with a resolution of 25cm appear rough, while there is no obvious difference in results with 10cm or 5cm resolution.

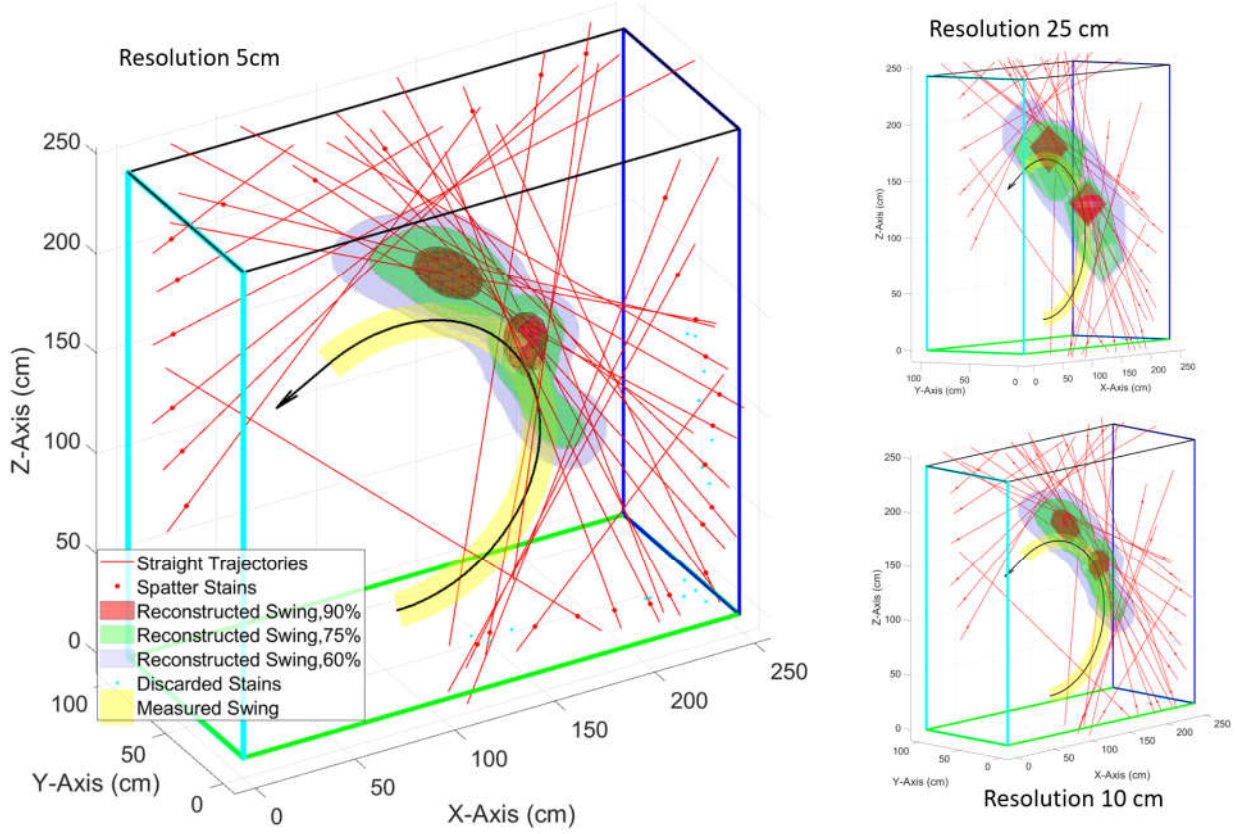

Figure 7: Reconstruction of the weapon swing in the "sitting" cast-off pattern. Comparison of reconstructed swings (red, green, blue volumes respectively correspond to to likelihood of 90%, 75% or 60%. The measured cast-off swing is the black arrow, with its measurement uncertainty in yellow. The same experimental cast-off data is reconstructed using three spatial resolutions: 25 cm, 10 cm and 5 cm.

Figure 8 displays the reconstruction results for non-circular "human" cast-off spatter (trial 7). Cast-off reconstruction results are superimposed with the corresponding captured cast-off motion depicted by a black line and uncertainty region in yellow, and video frames of the human subject producing the cast-off. The measured weapon swing was clockwise and clearly intersects the reconstructed regions.

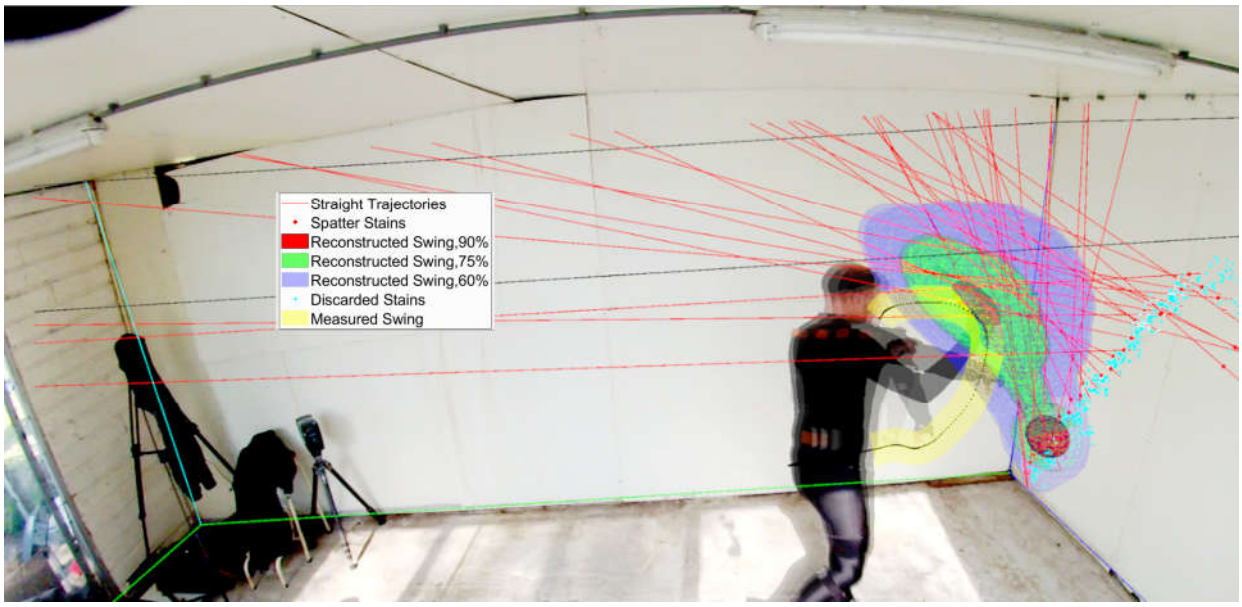

Figure 8: Cast-off reconstruction of trajectories for non-circular "Human" cast-off spatter pattern, trial 7. Comparison of reconstructed swing (red, green, blue volumes respectively correspond to reconstructions uncertainties of $U_{90\%}, U_{75\%}$ and $U_{60\%}$. The measured cast-off swing is the black arrow, with its measurement uncertainty in yellow. Simulation results, video motion pictures and accelerometer-based weapon swing measurements are superimposed, using the software CloudCompare.

For all the numerical results above, specific likelihood values have been specifically selected to minimize both uncertainty and error in the reconstruction. While the volume of the reconstructed swings is the uncertainty on the reconstruction of the weapon motion (which is a one-dimensional curved line, with zero volume), the error in the reconstructed cast-off region can be measured as the closest distance between the estimated reconstructed cast-off region and the recorded cast-off motion. We assume that the latter, within its own measurement uncertainty, is the most accurate measurement of the swing. Figure 9 illustrates how the uncertainty and error vary with the selected likelihood value, showing average values and standard deviations for the reconstruction of six *human* cast-off spatter patterns, similar to and including that of Figure 8. The average volume of each uncertainty region is provided in Figure 9, as a function of the likelihood value. The volume of the uncertainty region corresponding to likelihood $L = 90\%$, noted $U_{90\%}$, is smaller than 20*L* (the volume of a small daypack) for every one of the trials studied. Among all trials, the average uncertainty volumes $U_{75\%}$ and $U_{60\%}$ is respectively 104 *L* and 296 *L*, respectively. The lower the likelihood value, the larger the volume of the uncertainty region, until it becomes comparable to the volume of the entire room volume (58430 *L*). As reported in Figure 9, the average error associated with region $U_{90\%}$ is 6 cm, and the error is less than 17 cm for all the trials studied. The average error associated with $U_{75\%}$ for all trials is less than 2 cm. No error is found for $U_{60\%}$, which means that this uncertainty region embed at least a portion of the known cast-off motion for every trial considered. The choice of likelihood value therefore controls the trade-off between uncertainty and error. The lower the likelihood value, the lower the error, but the larger the uncertainty. The sweet spot of this trade-off is observed between *L* = 60% (where error is typically zero and uncertainty is reasonably small), and L = 90% (where uncertainty is minimal and error is about 10 cm). Thus, all the reconstruction results in this study are represented with three likelihood values of *L*=60%, 75% and 90%.

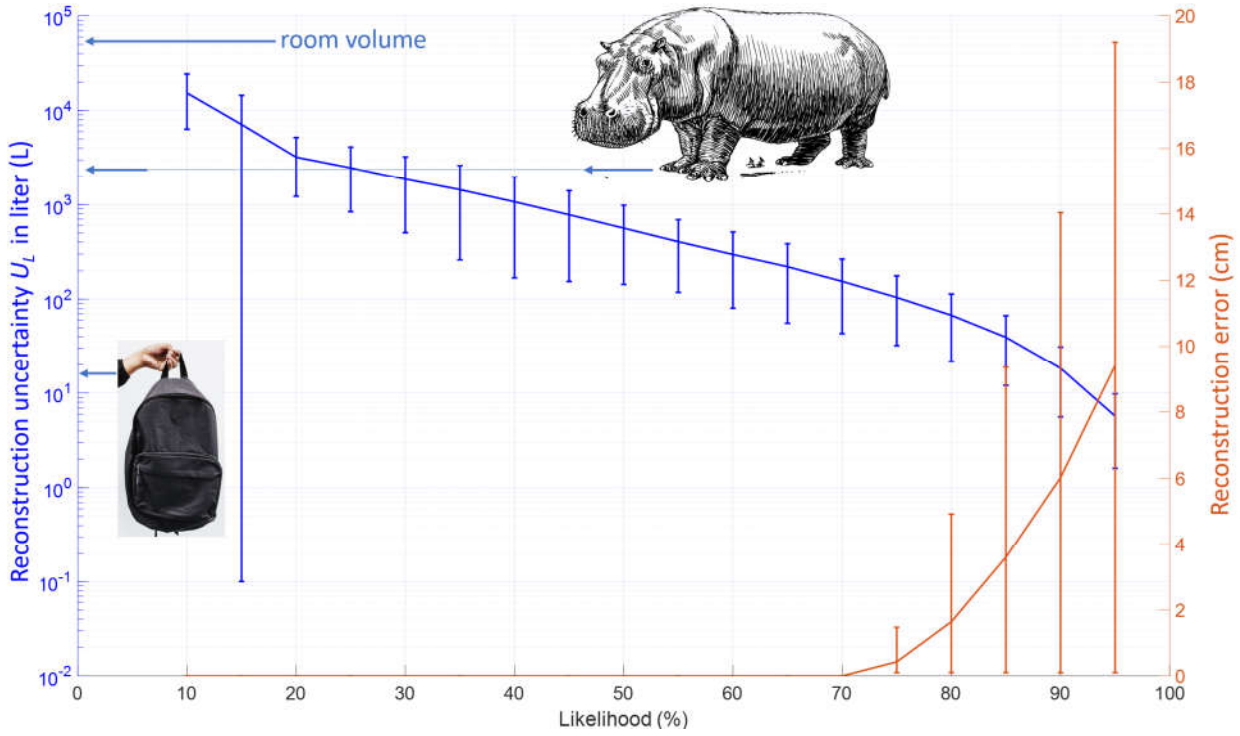

Figure 9: Trade-off between uncertainty and error in the reconstruction of the six *Human* cast-off trials, as a function of the likelihood value. The uncertainty is the volume of the reconstructed region, while the error is the closest distance between the recorded motion of the bloody object and the reconstructed region. Standard deviations among the trials is indicated by vertical bars. Images of hippopotamus and daypack are volume references to the reader, as is the volume of the room.

Figure 10 illustrates how the uncertainty in the reconstruction results increase with the uncertainty on stain measurement. Stain width and length can be measured within 0.1 mm uncertainty with state-of-the-art cameras. However, historical cases or crime scene videos typically provide lower resolution images, and the uncertainty on the stain size can be as large as 1 mm. The reconstructed swings in Figure 10 exhibit larger volumes for larger uncertainty on the measurement of the stain. This trend is both reasonable and an illustration that the reconstruction results depend on the quality of the input pictures. The fact that Human cast-off #7 can be reconstructed assuming both values of stain measurement uncertainty is also a sign of the robustness of the reconstruction method. Ultimately, a reconstruction method should propagate the uncertainties on the input data (here the stain measurements), as done for other types of bloodstain pattern analysis reconstruction [12, 33]. This is technically achieved here with the spread of the likelihood increasing with stain measurement uncertainty, as shown in Eq. (2).

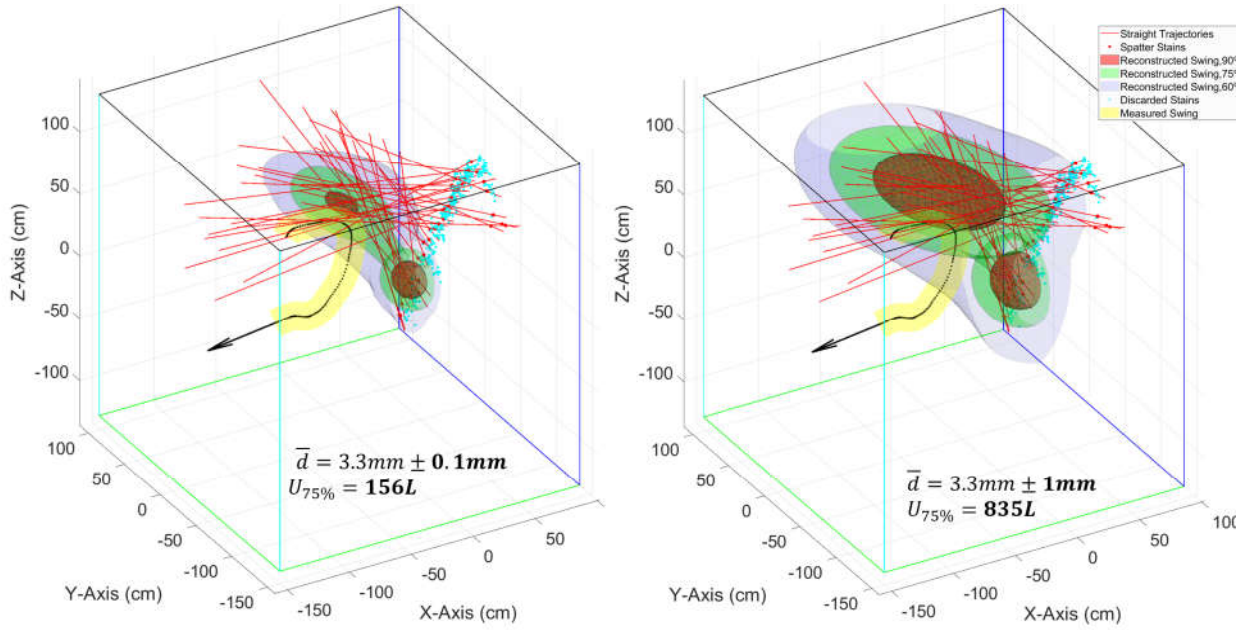

Figure 10: Effect of the quality of the stain measurement on the reconstruction results of *Human* castoff spatter pattern #7. Stains with equivalent diameter of 3.3 mm have been measured from high-quality photographs, corresponding to an uncertainty on the width and length of the stain of 0.1 mm. On the right, the same spatter pattern reconstructed with 1 mm uncertainty in the width and length of the stain, as would be with lower resolution crime scene pictures. Reconstruction for stains measured with more uncertainty exhibit a larger uncertainty as seen with the larger volumes of the reconstructed regions. Error in both cases is zero: the reconstructed region intersects with the measured weapon swing.

Every numerical method produces results that are sensitive to the spatial discretization, so it is important to perform the reconstruction with enough spatial discretization to make discretization errors negligible. Here, the space is discretized in cubes with side length *r,* oriented along the three main coordinates. In Figure 7, significant differences in the shape of the reconstructed regions are visible between the reconstructed regions with r = 25 cm or 10 cm; the former appearing rougher than the latter. We also measured that the larger the value of r, the larger the volumes of the uncertainty regions. For instance, r = 30 cm would give uncertainty volumes 21% larger than those for r=3 cm (the smallest resolution we have tested). Volumes of the uncertainty regions agreed within 10% for resolutions $r \leq 7$ cm, and within 5 % for $r \leq 5$ cm, with no observable significant difference in the shape between regions with $r \leq 7$ cm. Results presented in this study have thus been obtained with a spatial resolution r=5cm, unless otherwise specified. Computing time varied linearly with the volume of the space investigated, and was proportional to r^{-5}. Typical reconstruction simulation times on a recent laptop (Intel I7 2.4GHz processor) took 20 minutes with r = 5cm, and 25 seconds with r = 20 cm. The latter resolution is adequate for investigative work, suggesting that the method is suitable for real-time crime scene processing.

To further assess the capabilities of the reconstruction method, arbitrary spatter patterns have been numerically generated using geometrical intersections between the tangents to prescribed circles and the walls of a room. The prescribed swings (in black) and the corresponding reconstruction are in Figure

11. It appears that the reconstruction method can help distinguishing multiple swings from each other, such as circular swings in parallel planes (a) or in intersecting planes (b); The method is also able to reconstruct cast-off patterns where the swing has various orientations with respect to the vertical plane (b).

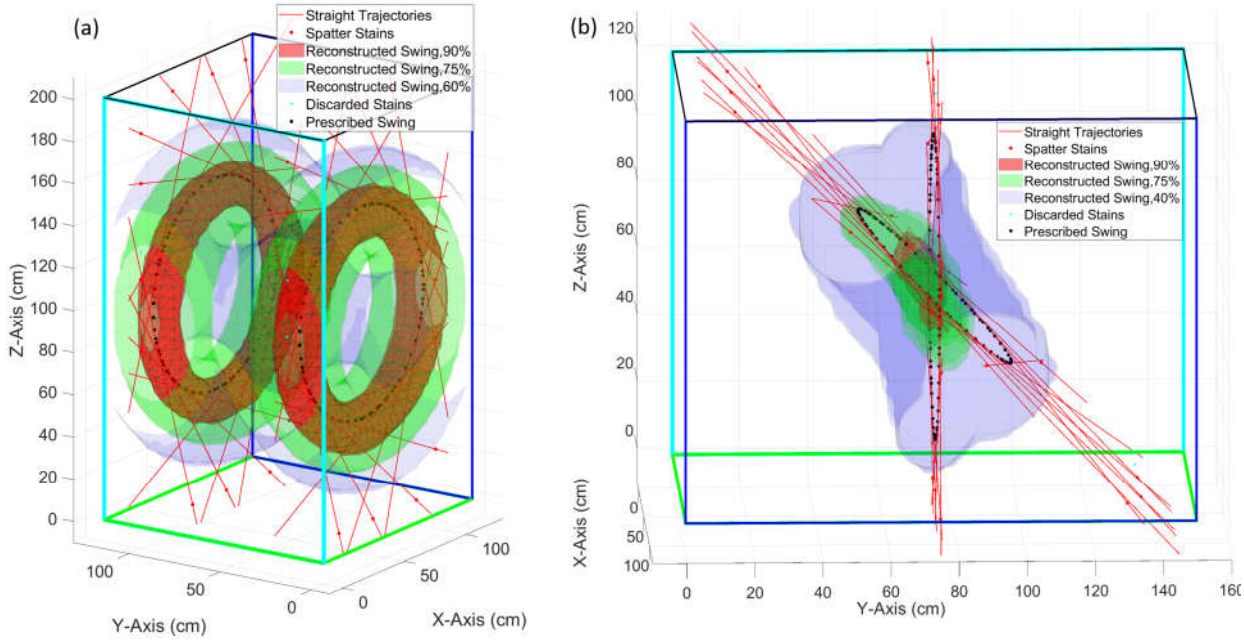

Figure 11: Ability of the algorithm to reconstruct spatter patterns produced by more than one cast-off swing event. Reconstruction of numerically generated stains prescribed by two circular swings that are either adjacent (a) and intersecting (b).

Implications for crime scene reconstruction.

This work provides a new tool to process crime scenes involving linear spatter patterns characteristic of cast-off events. The proposed tool can handle stains located on four perpendicular surfaces such as the walls of a room. The reconstruction results are provided with an uncertainty that is specific to the spatter pattern at hand. Best reconstruction results are produced using all the available stains, independently of size or ellipticity (see section 3.2). While round stains are usually avoided for area of origin determinations, since they imply large directional uncertainty [12], the proposed method automatically associates less weight to reconstructed arcs associated with round stains. According to the trade-off between uncertainty and error presented in Figure 9, likelihood values ranging from $60 \leq L < 90\%$ are recommended for investigative work. Spatial resolution of *r* =20 cm or less and pictures with less than 0.1 mm uncertainty on stain size are recommended for investigative work.

While the current model can be applied to current and historical forensic cases, there is room for future work. First, the presented method assumes straight-line trajectories of the drops. While this assumption can cause significant errors in the reconstruction of impact spatter patterns (which can be generated by drops with wide range of sizes and initial velocities), it is not clear at present how much error in cast-off reconstruction occurs by assuming straight trajectories. Certainly, the generation mechanism of cast-off is different than impact spatter patterns and may produce different distributions of drops sizes and

velocities, that may be less subject to deviation by drag and gravity. This hypothesis is however a topic of further studies. What is currently known is that reconstruction uncertainties associated with drag and gravity strongly depend on the distance between wall and origin, increasing with a power of about five of that distance [18]. Thus, analysts should be wary of reconstruction results where the reconstructed swing or area of origin are not close to the wall, a finding supported by experiments in [14]. Further studies may also extend the software capabilities to handle stains on walls of arbitrary orientations. It is also the first time that the authors propose a new reconstruction method as an open-source software, with the hope that forensic researchers will use it and provide feedback and input for future development.

Conclusions

In this manuscript, a method to reconstruct the motion, or swing, of a weapon generating cast-off stains has been proposed, based on stain inspection and Euclidean geometry. Agreement between measured and reconstructed swings is characterized in terms of error and uncertainty, and found to be very good. The reconstruction method allows for consideration of stains on up to four surfaces (front, back, ceiling and ground) and more than five-hundred stains to be inputted. The reconstruction method is robust in the sense that it delivers meaningful results for a broad range of spatial resolution and for crime scenes documented with high- or low-quality pictures. Specifically, the uncertainty of the reconstructed results is specific to the quality of the pictures of the spatter stains: results will have less uncertainty if the stains are measured with more precision. The reconstruction software used in this study is implemented as a numerical code written in an open source language, provided in an open access repository. Opportunities for future work are presented.

The software and installation instructions are available at

https://github.com/scottres/CastoffReconstruction.git

Acknowledgment

DA, KDB and SMC acknowledge financial support from the Center for Statistics and Applications in Forensic Evidence (CSAFE), through Cooperative Agreement No. 70NANB15H176 between NIST and Iowa State University, which includes activities carried out at Carnegie Mellon University, University of California Irvine, and University of Virginia. DA also acknowledges financial support from Iowa State University, as well as computing support from Struo LLC, a scientific consulting company based in Ames IA. DA thanks his Iowa State University colleague Xuan Hien Nguyen for pointing out the Euclidean geometry proposition to him. EL would like to thank Independent Forensic Services (IFS) for their assistance and use of their facilities and resources in collecting the human created cast-off patterns.

Contribution of Authors

DA designed and led the project, and guided the development of the software and reconstruction method. EL performed “Castanova” and non-circular “Human” cast-off experiments, processed the related patterns and swing motions, and provided the data. S.MC designed and wrote the numerical code, and performed the “Sitting” cast-off spatter experiments. De Brabanter provided input on the statistical part of the code. Most of the manuscript was written by SMC and DA, who both interpreted the results. All authors contributed to and reviewed the final manuscript.

Supplementary Documentation:

A. Calculation of the spreading of the PDF.

The probability that a given point in space is associated with a reconstructed cast-off arc first depends on the shape of the three stains used to determine the impact and directional angles. It is known that impact angles determined from round stains exhibit more uncertainty than angles obtained from very elliptical stains [12]. These angles are shown in Figure 2 as the impact angle α of each stain, and the directional angle γ of each stain.

Directional angle γ is defined as the angle between the main direction of the stain and a reference vector tangent to the stained surface, either the negative Z-direction or positive X-direction. Propagation of uncertainties on the measured shape of each stain associated with a given triplet n, provides an uncertainty δ_n.

The impact angle, $\alpha = \sin^{-1}\left(\frac{width}{length}\right)$, is estimated from the width and the length of an ellipse fitted on the stain, as in Figure 2. Uncertainties in the impact angles α of individual stains *k* of triplet n are estimated by propagation of the uncertainty on the stain measurement [12, 34],

$$\delta\alpha_{nk} = \frac{sin^2\alpha_{nk}}{1-sin^2\alpha_{nk}}\left[(1+sin^2\alpha_{nk})\frac{\sigma^2}{width_{nk}{}^2}\right], \quad \text{Eq. (5)}$$

where σ is the standard deviation of the width measurement. Uncertainties of round stains with ellipticities equal to one are maximum, while impact angles and ellipticities tending towards zero lead to minimal variance.

The total uncertainty on alpha for a given triplet *n* of stains in degrees, $\delta\alpha_n$, is estimated as the root mean square of the uncertainty on alpha of the three individual stains

$$\delta\alpha_n = \sqrt{\frac{\sum_{k=1}^{3}\delta\alpha_{nk}^2}{3}}. \quad \text{Eq. (6)}$$

The uncertainty on the directional angle γ, $\delta\gamma_{nk}$, is estimated as in Attinger [18]. In degrees, we have

$$\delta\gamma_{nk} = 0.42e^{0.054\alpha_{nk}}. \quad \text{Eq. (7)}$$

This uncertainty on γ is maximum for round stains, and minimum for elongated stains.

The total uncertainty on γ for triplet *n* is determined using the classical root mean square (RMS) formula.

$$\delta\gamma_n = \sqrt{\frac{\sum_{k=1}^{3}\delta\gamma_{nk}^2}{3}} \quad \text{Eq. (8)}$$

For a given triplet, the magnitude $\bar{\alpha}$ of the angular uncertainty due to the stain shape is expressed as the root mean square of the uncertainties on the determination of impact angle $\alpha_n$and directional angle γ_n, as

$$\bar{\alpha} = \sqrt{\frac{\delta\alpha_n^2 + \delta\gamma_n^2}{2}}. \quad \text{Eq. (9)}$$

The second parameter in Eq. (3) is $\overline{\varphi}$, an angle measuring the alignment of the three impact velocities associated with the triplet of stains and the best-fit plane containing the reconstructed arc. Angle $\overline{\varphi}$ is estimated as the root mean square of the angle between the three impact velocities and the best-fit plane.

The third parameter in Eq. (3) is Δ_{wall}, the root mean square of the distances between the three stains and the reconstructed arc.

Finally, we use the trigonometric definition of the tangent to construct the function fulfilling the relation postulated by Eq. (3), as

$$SF_{jn} = \Delta_{wall}\sqrt{\tan^2(\bar{\alpha}) + \tan^2(\overline{\varphi})}\,.$$

B. Cast-off Reconstruction Program Inputs

This section describes the inputs used in the numerical simulations, with their magnitude and definition.

Table 2: User defined variable inputs with operating range and default magnitudes.

Input (with name in the code)	**Magnitude Range**	**Default Magnitude**	**Physical Definition**
Resolution, *res*	$[1-15]$ cm	5 cm	Resolution of Heat Map (Length of Regions in Space Cube Dimensions). Finer resolutions are preferred but may exceed 'Maximum Possible array' or memory capabilities.
Likelihood Values, *percentiles*	$[0-100]$ %	$[90, 75, 60]$ %	Likelihood value used to estimate the volume and uncertainty of the reconstructed weapon swing. Likelihood values $L \geq 60\%$ are used to minimize the uncertainty in the reconstructed cast-off motion.
Standard Deviation, *stdev*	$[0.001-1]$ mm	0.1 mm	Approximated standard deviation in the measurement of the stain width. Depends on the quality of the casework images and on the measurement method.

C. **Defining Euclidean Vector Components of Impact Velocity:**

Consider as in Figure 2 a vector n normal to the surface directed out of the room and tangential vector t is the gravity vector within the surface plane defined for each surface. The tangential vector is redefined in the positive *x*-direction for horizontal surfaces since the tangential vector is normal to the surface. The normal vectors for the back, upward, front, and downward surfaces are then as follows, $n_1 = [1,0,0]$, $n_2 = [0,0,1]$, $n_3 = [-1,0,0]$, and $n_4 = [0,0,-1]$ and tangential vectors $t_1 = [0,0,-1]$, $t_2 = [0,0,-1]$, $t_3 = [0,0,-1]$, and $t_4 = [0,0,-1]$. The orthogonal vector to n and t is the cross product of the two vectors, $n \times t$, which gives us $(n \times t)_1 = [0,0,-1]$, $(n \times t)_2 = [1,0,0]$, $(n \times t)_3 = [0,0,-1]$, and $(n \times t)_4 = [1,0,0]$.

The normal, tangential, and orthogonal vectors relate each surface stain impact angle to determine the Euclidean components of the stain trajectory vectors. The following equations, derived from [35], relate measured impact angles to normalized stain trajectory vectors.

$$v_{n_i} = n_i \cdot \sin\alpha \, ; v_{n \times t_i} = (n \times t)_i \cdot \frac{1}{tan\beta} \quad \text{Eq. (10)}$$

$$v_{t_i} = t_i \cdot \frac{1}{tan\gamma} \quad \text{Eq. (11)}$$

$$v_i = \left[v_{n_i} + v_{n \times t_i} + v_{t_i}\right] = \left[v_x, v_y, v_z\right] \quad \text{Eq. (12)}$$

D. Application of the Pratt fit method

The Pratt fit method is used to identify which one of three escribed circles associated with any given triplet of stains as in Figure 3 is relevant to the reconstruction of a cast-off arc. All combinations and permutations of drop trajectories are considered to ensure all possible trajectory intersections are fitted using the Pratt fit method. These combinations and permutations of stain trajectory endpoints are obtained and compiled, $\binom{n}{r} = \frac{n!}{r!(n-r)!}$ where n is the number of unique stain trajectory elements of size r, such that each pair of nonparallel trajectories has one intersection point. The Pratt fit method is a simple algebraic relation between a circle's radius and algebraic circle parameter A with constraints $A \neq 0$ and $B^2 + C^2 - 4AD > 0$. This relation, Eq. (13) can be rewritten as Eq. (14) and numerically solved [31]. The Pratt fit method produces a circle center location (x_i, y_i) and radius R that minimizes $\mathcal{F}(A, B, C, D) = \sum \left[\frac{1}{4R^2} \frac{[Az_i + Bx_i + Cy_i + D]^2}{B^2 + C^2 - 4AD}\right]$ where $z_i = x_i^2 + y_i^2$ [31].

$$A(x^2 + y^2) + Bx + Cy + D = 0 \qquad \text{Eq. (13)}$$

$$\left(x - \frac{B}{2A}\right)^2 + \left(y - \frac{C}{2A}\right)^2 - \frac{B^2 + C^2 - 4AD}{4A^2} = 0 \qquad \text{Eq. (14)}$$

References

[1] "ASB Technical Report 033, Terms and Definitions in Bloodstain Pattern Analysis," Academy Standards BoardFirst Edition, 2017.

[2] E. M. P. Williams, E. S. Graham, M. C. Jermy, D. C. Kieser, and M. C. Taylor, "The Dynamics of Blood Drop Release from Swinging Objects in the Creation of Cast-off Bloodstain Patterns," (in English), *Journal of Forensic Sciences,* Article vol. 64, no. 2, pp. 413-421, Mar 2019.

[3] R. M. Arthur, J. Hoogenboom, M. Baiker, M. C. Taylor, and K. G. De Bruin, "An automated approach to the classification of impact spatter and cast-off bloodstain patterns," *Forensic Science International,* vol. 289, pp. 310-319, 2018.

[4] C. D. Adam, "Experimental and theoretical studies into the release of blood droplets from weapon tips," (in English), *Forensic Science International,* Article vol. 303, p. 11, Oct 2019, Art. no. 109934.

[5] D. Attinger, C. Moore, A. Donaldson, A. Jafari, and H. A. Stone, "Fluid dynamics topics in bloodstain pattern analysis: Comparative review and research opportunities," *Forensic Science International,* vol. 231, no. 1-3, pp. 375-396, Sep 2013.

[6] N. Kabaliuk, M. C. Jermy, E. Williams, T. L. Laber, and M. C. Taylor, "Experimental validation of a numerical model for predicting the trajectory of blood drops in typical crime scene conditions, including droplet deformation and breakup, with a study of the effect of indoor air currents and wind on typical spatter drop trajectories," (in English), *Forensic Science International,* Article vol. 245, pp. 107-120, Dec 2014.

[7] S. N. Kunz, J. Adamec, and C. Grove, "Analyzing the Dynamics and Morphology of Cast-off Pattern at Different Speed Levels Using High-speed Digital Video Imaging," (in English), *Journal of Forensic Sciences,* Article vol. 62, no. 2, pp. 428-434, Mar 2017.

[8] T. Raymond, "Crime Scene Reconstruction from Bloodstains," *Australian Journal of Forensic Sciences,* vol. 29, no. 2, pp. 69-78, 1997/07/01 1997.

[9] E. M. P. T. Williams, Michael, "The Development and Construction of a Motorized Blood Droplet Generation Device (BDGD), for Detailed Analysis of Blood Droplet Dynamics," *Journal of Bloodstain Pattern Analysis,* vol. 29, 2013.

[10] N. Behrooz, L. Hulse-Smith, and S. Chandra, "An Evaluation of the Underlying Mechanisms of Bloodstain Pattern Analysis Error," *Journal of Forensic Sciences,* vol. 56, no. 5, pp. 1136-1142, Sep 2011.

[11] U. Buck, B. Kneubuehl, S. Nather, N. Albertini, L. Schmidt, and M. Thali, "3D bloodstain pattern analysis: Ballistic reconstruction of the trajectories of blood drops and determination of the centres of origin of the bloodstains," (in English), *Forensic Science International,* Article vol. 206, no. 1-3, pp. 22-28, Mar 2011.

[12] F. Camana, "Determining the area of convergence in Bloodstain Pattern Analysis: A probabilistic approach," *Forensic Science International,* vol. 231, no. 1-3, pp. 131-136, Sep 10 2013.

[13] A. L. Carter, "The Directional Analysis of Bloodstain Patterns Theory and Experimental Validation," *Canadian Society of Forensic Science Journal,* vol. 34, no. 4, pp. 173-189, 2001/01/01 2001.

[14] K. G. de Bruin, R. D. Stoel, and J. C. M. Limborgh, "Improving the Point of Origin Determination in Bloodstain Pattern Analysis," *Journal of Forensic Sciences,* vol. 56, no. 6, pp. 1476-1482, Nov 2011.

[15] N. Hakim and E. Liscio, "Calculating Point of Origin of Blood Spatter Using Laser Scanning Technology," (in English), *Journal of Forensic Sciences,* Article vol. 60, no. 2, pp. 409-417, Mar 2015.
[16] E. Liscio, P. Bozek, H. Guryn, and Q. Le, "Observations and 3D Analysis of Controlled Cast-Off Stains," *J Forensic Sci,* Feb 18 2020.
[17] A. C. Maloney, T.; Killeen, J., "Visualization of Cast-off Patterns Using 3D Modelling Software," *Journal of the Association for Crime Scene Reconstruction,* vol. 17, no. 4, pp. 49-56, 2011.
[18] D. Attinger, P. M. Comiskey, A. L. Yarin, and K. De Brabanter, "Determining the region of origin of blood spatter patterns considering fluid dynamics and statistical uncertainties," (in English), *Forensic Science International,* Article vol. 298, pp. 323-331, May 2019.
[19] U. Windberger, A. Bartholovitsch, R. Plasenzotti, K. J. Korak, and G. Heinze, "Whole blood viscosity, plasma viscosity and erythrocyte aggregation in nine mammalian species: reference values and comparison of data," *Experimental Physiology,* vol. 88, no. 3, pp. 431-440, 2003.
[20] D. Attinger, Y. Liu, and K. De Brabanter, "Authors' Response," *J Forensic Sci,* Jun 8 2020.
[21] D. Attinger, Y. Liu, T. Bybee, and K. De Brabanter, "A data set of bloodstain patterns for teaching and research in bloodstain pattern analysis: Impact beating spatters," (in English), *Data in Brief,* Article; Data Paper vol. 18, pp. 648-654, Jun 2018.
[22] E. Liscio, P. Bozek, H. Guryn, and Q. Le, "Observations and 3D Analysis of Controlled Cast-Off Stains," (in English), *Journal of Forensic Sciences,* Article; Early Access p. 13, 2020 2020.
[23] J. R. Peiro, A. S. Borges, R. C. Goncalves, and L. C. N. Mendes, "Evaluation of a portable clinical analyzer for the determination of blood gas partial pressures, electrolyte concentrations, and hematocrit in venous blood samples collected from cattle, horses, and sheep," (in English), *American Journal of Veterinary Research,* Article vol. 71, no. 5, pp. 515-521, May 2010.
[24] J. T. Zhang, A. C. Novak, B. Brouwer, and Q. G. Li, "Concurrent validation of Xsens MVN measurement of lower limb joint angular kinematics," (in English), *Physiological Measurement,* Article vol. 34, no. 8, pp. N63-N69, Aug 2013.
[25] M. Capecci, M. G. Ceravolo, F. Ferracuti, S. Iarlori, S. Longhi, L. Romeo, S. N. Russi, and F. Verdini, "Accuracy evaluation of the Kinect v2 sensor during dynamic movements in a rehabilitation scenario," in *2016 38th Annual International Conference of the Ieee Engineering in Medicine and Biology Society*, J. Patton *et al.*, Eds. (IEEE Engineering in Medicine and Biology Society Conference Proceedings, New York: Ieee, 2016, pp. 5409-5412.
[26] E. Lachat, H. Macher, M. A. Mittet, T. Landes, and P. Grussenmeyer, "FIRST EXPERIENCES WITH KINECT V2 SENSOR FOR CLOSE RANGE 3D MODELLING," in *3d-Arch 2015 - 3d Virtual Reconstruction and Visualization of Complex Architectures*, vol. 40-5, D. GonzalezAguilera, F. Remondino, J. Boehm, T. Kersten, and T. Fuse, Eds. (International Archives of the Photogrammetry Remote Sensing and Spatial Information Sciences, no. W4) Gottingen: Copernicus Gesellschaft Mbh, 2015, pp. 93-100.
[27] T. L. HEATH, *THE WORKS OF ARCHIMEDES*. 1897.
[28] R. Lachlan, ""The Inscribed and the Escribed Circles." §126-128 in An Elementary Treatise on Modern Pure Geometry," *London Macmillan,* pp. 72-74, 1893.
[29] A. V. Wouwer, P. Saucez, and C. Vilas, *Simulation of ODE/PDE Models with MATLAB, Octave and Scilab: Scientific and Engineering Applications*. Springer, 2014.
[30] H. S. M. Coxeter and S. L. Greitzer, *Geometry revisited*. New York: Mathematical Association of America, 1967.
[31] V. Pratt, "Direct Least-Squares Fitting of Algebraic Surfaces," *SIGGRAPH,* vol. 21, no. 4, pp. 145-152, April 30, 1987 1987.

[32] J. C. Lagarias, J. A. Reeds, M. H. Wright, and P. E. Wright, "Convergence Properties of the Nelder-Mead Simplex Method in Low Dimensions," *SIAM Journal of Optimization,* vol. 9, no. 1, pp. 112–147, 1998.

[33] D. Attinger, P. M. Comiskey, A. L. Yarin, and K. D. Brabanter, "Determining the region of origin of blood spatter patterns considering fluid dynamics and statistical uncertainties," *Forensic Science International,* vol. 298, pp. 323-331, 2019.

[34] C. Willis, A. K. Piranian, J. R. Donaggio, R. J. Barnett, and W. F. Rowe, "Errors in the estimation of the distance of fall and angles of impact blood drops," (in English), *Forensic Science International,* Article vol. 123, no. 1, pp. 1-4, Nov 2001.

[35] A. L. Carter, "The Directional Analysis of Bloodstain Patterns: Theory and Experimental Validation," *Journal of the Canadian Society of Forensic Science,* vol. 34, no. 4, pp. 173-173, 2001.